The Astrophysical Journal Letters, 779:L11 (7pp), 2013 December 10 doi:10.1088/2041-8205/779/1/L11

EINSTEIN@HOME DISCOVERY OF FOUR YOUNG GAMMA-RAY PULSARS IN *FERMI* LAT DATA

H. J. Pletsch[1,2], L. Guillemot[3,9], B. Allen[1,4,2], D. Anderson[5], C. Aulbert[1,2], O. Bock[1,2], D. J. Champion[3], H. B. Eggenstein[1,2], H. Fehrmann[1,2], D. Hammer[4], R. Karuppusamy[3], M. Keith[6], M. Kramer[3,7], B. Machenschalk[1,2], C. Ng[3], M. A. Papa[1,4], P. S. Ray[8], and X. Siemens[4]

[1] Max-Planck-Institut für Gravitationsphysik (Albert-Einstein-Institut), D-30167 Hannover, Germany; holger.pletsch@aei.mpg.de
[2] Institut für Gravitationsphysik, Leibniz Universität Hannover, D-30167 Hannover, Germany
[3] Max-Planck-Institut für Radioastronomie, Auf dem Hügel 69, D-53121 Bonn, Germany
[4] Department of Physics, University of Wisconsin–Milwaukee, Milwaukee, WI 53201, USA
[5] Space Sciences Laboratory, University of California, Berkeley, CA 94720, USA
[6] CSIRO Astronomy and Space Science, Australia Telescope National Facility, Australia
[7] Jodrell Bank Centre for Astrophysics, School of Physics and Astronomy, The University of Manchester, Manchester M13 9PL, UK
[8] Space Science Division, Naval Research Laboratory, Washington, DC 20375-5352, USA
Received 2013 September 6; accepted 2013 October 30; published 2013 November 26

ABSTRACT

We report the discovery of four gamma-ray pulsars, detected in computing-intensive blind searches of data from the *Fermi* Large Area Telescope (LAT). The pulsars were found using a novel search approach, combining volunteer distributed computing via Einstein@Home and methods originally developed in gravitational-wave astronomy. The pulsars PSRs J0554+3107, J1422−6138, J1522−5735, and J1932+1916 are young and energetic, with characteristic ages between 35 and 56 kyr and spin-down powers in the range 6×10^{34}—10^{36} erg s^{-1}. They are located in the Galactic plane and have rotation rates of less than 10 Hz, among which the 2.1 Hz spin frequency of PSR J0554+3107 is the slowest of any known gamma-ray pulsar. For two of the new pulsars, we find supernova remnants coincident on the sky and discuss the plausibility of such associations. Deep radio follow-up observations found no pulsations, suggesting that all four pulsars are radio-quiet as viewed from Earth. These discoveries, the first gamma-ray pulsars found by volunteer computing, motivate continued blind pulsar searches of the many other unidentified LAT gamma-ray sources.

Key words: gamma rays: stars – pulsars: general – pulsars: individual (PSRs J0554+3107, J1422−6138, J1522−5735, J1932+1916)

Online-only material: color figures

1. INTRODUCTION

The Large Area Telescope (LAT; Atwood et al. 2009) aboard the *Fermi Gamma-ray Space Telescope* has established pulsars as predominant Galactic gamma-ray sources at GeV energies (Abdo et al. 2013). Most LAT-detected gamma-ray pulsars have been unveiled *indirectly*. In these cases, known radio pulsar ephemerides are used to assign rotational phases to gamma-ray photons and probe for pulsations. Additionally, dedicated radio searches at positions of unidentified gamma-ray sources as in the *Fermi*-LAT Second Source Catalog (2FGL; Nolan et al. 2012) discovered many new radio pulsars, likewise providing ephemerides for gamma-ray phase-folding (e.g., Guillemot et al. 2012; Abdo et al. 2013).

For the first time, pulsars have also been detected in *direct* searches for periodicity in the sparse LAT gamma-ray photons (Abdo et al. 2009). In fact, many pulsars found in such "blind" searches are undetected at radio wavelengths (Ray et al. 2012; Abdo et al. 2013). Blind searches are computationally challenging, because the relevant pulsar parameters are unknown in advance (e.g., Chandler et al. 2001). The challenge is to search a dense grid covering a multidimensional parameter space (for isolated systems: sky location, frequency f, and spin-down rate $\dot{f}$). The number of grid points to be individually tested increases rapidly with coherent integration time (e.g., Brady et al. 1998): for observations spanning multiple years the finite computing power available makes blind searches with fully coherent ("brute-force") methods unfeasible, and much more *efficient* methods are essential.

During the first year of the *Fermi* mission, pioneering blind searches revealed 24 pulsars in LAT data (Abdo et al. 2009; Saz Parkinson et al. 2010) through a clever time-differencing technique (Atwood et al. 2006; Ziegler et al. 2008) that exploits that sparsity of the LAT data. Increasing data time spans intensify the computing burden, and only two more pulsars were found in the second year (Abdo et al. 2013). However, hundreds of unidentified LAT sources with pulsar-like properties (Ackermann et al. 2012; Lee et al. 2012) probably harbor undiscovered pulsars.

The blind-search problem is analogous to searches for continuous gravitational waves (GWs) emitted from spinning neutron stars (Brady et al. 1998), also called "GW pulsars." This similarity has motivated us to use data-analysis methods originally developed for GW-pulsar detection (Brady & Creighton 2000; Cutler et al. 2005; Pletsch & Allen 2009; Pletsch 2010, 2011) to significantly enhance the sensitivity of blind searches for gamma-ray pulsars.

Using these methods to search LAT data has led to the discovery of 10 new gamma-ray pulsars (Pletsch et al. 2012a, 2012c) on the *Atlas* computing cluster in Hannover. While these discoveries were isolated young pulsars (with spin frequencies of 3–12 Hz), the ongoing searches also cover the higher-frequency range of millisecond pulsars (MSPs). With partial orbital constraints from optical data (Romani 2012), these methods

[9] Currently at Laboratoire de Physique et Chimie de l'Environnement et de l'Espace–Université d'Orléans/CNRS, F-45071 Orléans Cedex 02, France; lucas.guillemot@cnrs-orleans.fr

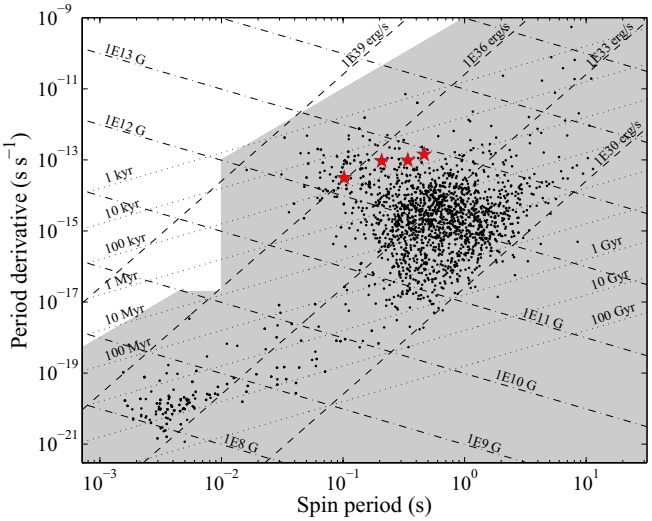

Figure 1. Period–period derivative diagram of the pulsar population. Filled stars show the four new gamma-ray pulsars. Black dots represent known radio pulsars from the ATNF catalog (Manchester et al. 2005). The gray shaded region indicates the search parameter space. Dotted lines indicate contours of constant τ_c; similarly, dashed lines show spin-down power $\dot{E}$ and dashed-dotted lines refer to surface magnetic field strength B_S.

(A color version of this figure is available in the online journal.)

also discovered a binary MSP via gamma-ray pulsations (Pletsch et al. 2012b).

Searching for fast spinning isolated MSPs dominates the overall computing cost of this survey. To enlarge the available computational resources we have recently moved the survey onto the volunteer computing system Einstein@Home.[10] Here, we present the Einstein@Home discovery and key parameters of four young, energetic pulsars, PSR J0554+3107, PSR J1422−6138, PSR J1522−5735, and PSR J1932+1916, detected in the ongoing blind survey of unidentified LAT sources. These are the first gamma-ray pulsars discovered using volunteer computing.

2. SURVEY AND PULSAR DISCOVERIES

The survey targets unidentified 2FGL sources with properties reminiscent of known pulsars. Such selection criteria include significantly curved emission spectra and low flux variability over time (Ackermann et al. 2012), leading to a list of 109 2FGL sources (Pletsch et al. 2012a). Further details on source selection and data preparation are described in Pletsch et al. (2012a).

For each selected target source, a blind search for isolated gamma-ray pulsars has been carried out in 3 yr of LAT data. The parameter space of the search is four-dimensional (sky position, spin-frequency f, and $\dot{f}$). In the sky, a circular region is searched, centered on the 2FGL-catalog source location having a radius 20% larger than the semi-major axis of the 95% confidence elliptical error region. The survey covers an f range up to 1.4 kHz, in order to be sensitive to MSPs. For $f \geqslant 100$ Hz, spin-down rates in the range -1×10^{-12} Hz s^{-1} $\leqslant \dot{f} \leqslant 0$ are searched (see Figure 1). To maintain sensitivity to young pulsars, for $f < 100$ Hz the $\dot{f}$ search range is extended down to characteristic ages $\tau_c = -f/2\dot{f} \sim 1$ kyr, comparable to that of the Crab pulsar.

The data-analysis strategy employed in the blind search follows a hierarchical (multistage) approach, outlined in Pletsch et al. (2012a). The first stage explores the full parameter space with an efficient semi-coherent method: coherent Fourier powers computed with a ≈6 day window are incoherently summed as the window slides along the entire data set. A parameter-space metric (Pletsch & Allen 2009; Pletsch 2010; Pletsch et al. 2012a) is used to build an efficient search grid. In the second stage, only significant semi-coherent candidates are followed up via a fully coherent analysis. A third stage further refines coherent pulsar candidates by using higher signal harmonics (adopting the H-test of de Jager et al. 1989).

The Einstein@Home volunteer supercomputer does the bulk of the computational work. Einstein@Home was launched in 2005 to search for GW pulsars in detector data from the LIGO–VIRGO Collaboration (Abbott et al. 2009b, 2009a; Aasi et al. 2013). Since 2009, Einstein@Home has also been analyzing radio telescope data, finding several new radio pulsars (Knispel et al. 2010, 2011, 2013; Allen et al. 2013). In parallel, Einstein@Home is now also searching for gamma-ray pulsars as described here. This extends the radio and GW efforts with a third distinct search for new neutron stars.

To sign up for Einstein@Home, members of the general public download free software for their Windows, Apple, or Linux computers or Android device. Working in the background, the software automatically downloads work units (executables and data) from the Einstein@Home servers, carries out a search when the host machine is idle, and reports back results. Returned results are automatically validated by comparison of the outcome for the same work unit produced by a different volunteer's host. With more than 300,000 individuals already contributing, the sustained computing capacity achieved (1 PFlop/s) is comparable with the world's largest supercomputers.

The Einstein@Home results for the formerly unidentified LAT sources, 2FGL J0553.9+3104, 2FGL J1422.5−6137c, 2FGL J1521.8−5735, and 2FGL J1932.1+1913, indicated significant pulsations. All but one of these sources also have counterparts in the *Fermi* LAT First Source Catalog (1FGL; Abdo et al. 2010), denoted by 1FGL J0553.9+3105, 1FGL J1521.8−5734c, and 1FGL J1932.1+1914c. A dedicated follow-up investigation to further refine the parameters and properties of the newly discovered pulsars is described below.

3. THE FOUR GAMMA-RAY PULSARS

For follow-up analysis, we extended the original data sets to include LAT photons recorded from 2008 August 4 until 2013 April 1. We used the *Fermi* Science Tools[11] (STs) to select "Source"-class photons according to the P7_V6 instrument response functions (IRFs), with reconstructed directions within 15° of the pulsars, energies above 100 MeV, and zenith angles ⩽100°. We excluded photons recorded when the LAT's rocking angle exceeded 52°, or when the LAT was not in nominal science mode. We assigned each photon a weight measuring the probability of having originated from the pulsar (as was also done for the search). These weights (Kerr 2011) were computed with *gtsrcprob* based on a spectral model of the region (described below) and the LAT IRFs. This photon-weighting scheme improves the signal-to-noise ratio of the pulsations, providing better background rejection than simple angular and energy cuts.

[10] http://einstein.phys.uwm.edu/

[11] http://fermi.gsfc.nasa.gov/ssc/data/analysis/scitools/overview.html

Table 1
Measured and Derived Pulsar Parameters

Parameter	PSR J0554+3107	PSR J1422−6138	PSR J1522−5735	PSR J1932+1916
Right ascension, α (J2000.0)	$05^h54^m05\overset{s}{.}01(3)$	$14^h22^m27\overset{s}{.}07(1)$	$15^h22^m05\overset{s}{.}3(1)$	$19^h32^m19\overset{s}{.}70(4)$
Declination, δ (J2000.0)	$+31°07'41''(4)$	$-61°38'28''(1)$	$-57°35'00''(1)$	$+19°16'39''(1)$
Galactic longitude, l (°)	179.1	313.5	322.1	54.7
Galactic latitude, b (°)	2.70	−0.66	−0.42	0.08
Spin frequency, f (Hz)	2.15071817570(7)	2.932827817(1)	9.790868913(3)	4.8027301667(3)
Frequency first derivative, $\dot{f}$ (10^{-12} Hz s^{-1})	−0.659622(5)	−0.83293(9)	−2.9946(2)	−2.14916(1)
Frequency second derivative,[a] $\ddot{f}$ (10^{-23} Hz s^{-2})	0.18(2)	−1.5(3)	−2.6(5)	−0.3(1)
Epoch (MJD)	55214	55214	55250	55214
Weighted H-test (single-trial false alarm probability)	425($\sim 10^{-80}$)	469($\sim 10^{-89}$)	319($\sim 10^{-59}$)	460($\sim 10^{-87}$)
Epoch of glitch 1 (MJD)	-	55310	55250	-
Permanent f increment, $\Delta f_{\mathrm{glitch\,1}}$ (10^{-6} Hz)	-	0.026528575(2)	−0.112(6)	-
Permanent $\dot{f}$ increment, $\Delta \dot{f}_{\mathrm{glitch\,1}}$ (10^{-15} Hz s^{-1})	-	6.4(4.8)	3.6(4)	-
Decaying f increment, $\Delta f_{d,\mathrm{glitch\,1}}$ (10^{-6} Hz)	-	-	0.42(6)	-
Decay time constant, $\tau_{d,\mathrm{glitch\,1}}$ (days)	-	-	27(5)	-
Epoch of glitch 2 (MJD)	-	55450	-	-
Permanent f increment, $\Delta f_{\mathrm{glitch\,2}}$ (10^{-6} Hz)	-	1.18798307(4)	-	-
Permanent $\dot{f}$ increment, $\Delta \dot{f}_{\mathrm{glitch\,2}}$ (10^{-15} Hz s^{-1})	-	−5.3(5.0)	-	-
Characteristic age, τ_c (kyr)	51.7	55.8	51.8	35.4
Spin-down power, $\dot{E}$ (10^{34} erg s^{-1})	5.6	9.6	115.7	40.7
Surface magnetic field strength, B_S (10^{12} G)	8.2	5.8	1.8	4.5
Light-cylinder magnetic field strength, B_{LC} (kG)	0.8	1.3	15.6	4.5
Estimated maximum distance,[b] $d_{100\%}$ (kpc)	$\lesssim 5.2$	$\lesssim 4.8$	$\lesssim 12.5$	$\lesssim 6.6$
Estimated "heuristic" distance,[c] d_h (kpc)	~ 1.9	~ 1.5	~ 2.1	~ 1.5
Spectral index, Γ	1.1 ± 0.2	0.3 ± 0.2	1.4 ± 0.2	1.7 ± 0.1
Cutoff energy, E_c (GeV)	1.3 ± 0.2	2.5 ± 0.3	1.5 ± 0.3	1.2 ± 0.2
Photon flux above 100 MeV, F_{100} (10^{-8} photons cm^{-2} s^{-1})	1.9 ± 0.3	1.1 ± 0.2	8.5 ± 1.1	15.1 ± 1.0
Energy flux above 100 MeV, G_{100} (10^{-11} erg cm^{-2} s^{-1})	1.7 ± 0.1	3.5 ± 0.3	6.2 ± 0.4	7.8 ± 0.4
Peak multiplicity	3	2	1	1
$\mathrm{FWHM}_{\mathrm{Peak\,1}}$	0.10 ± 0.02	0.12 ± 0.02	0.22 ± 0.02	0.23 ± 0.03
$\mathrm{FWHM}_{\mathrm{Peak\,2}}$	0.06 ± 0.02	0.11 ± 0.01	-	-
$\mathrm{FWHM}_{\mathrm{Peak\,3}}$	0.03 ± 0.01	-	-	-
Peak 1 to 2 separation	0.24 ± 0.01	0.18 ± 0.01	-	-
Peak 1 to 3 separation	0.35 ± 0.01	-	-	-
Radio-flux-density upper limit at 1.4 GHz, S_{1400} (μJy)	66	60	34	75

Notes. The data time span is 54702–56383 MJD. The JPL DE405 solar system ephemeris has been used; times refer to Barycentric Dynamical Time. Numbers in parentheses are statistical 1σ errors in the last digits.

[a] Parameterizes timing noise (and glitch recovery where applicable) rather than pulsar intrinsic spin-down.

[b] Assuming 100% efficiency ($L_\gamma = \dot{E}$) and $f_\Omega = 1$, gives rise to $d_{100\%} = (\dot{E}/4\pi\, G_{100})^{1/2}$.

[c] Assuming a "heuristic" luminosity $L_\gamma^h = (\dot{E}/10^{33}\ \mathrm{erg\ s^{-1}})^{1/2}\ 10^{33}$ erg s^{-1} and $f_\Omega = 1$, yields $d_h = (L_\gamma^h/4\pi\, G_{100})^{1/2}$.

With these LAT data sets, we refined the initial pulsar parameters after discovery, using the methods by Ray et al. (2011). We subdivided the data sets into segments of about equal length and produced pulse profiles for all segments by folding the photon times with the initial parameters. These pulse profiles were correlated with "template" profiles to obtain pulse times of arrival (TOAs). Using Tempo2 (Hobbs et al. 2006) we fitted the TOAs to a timing model with sky position, frequency, and frequency derivatives. Table 1 presents the best-fit timing solutions.

For two of the pulsars, PSRs J1422−6138 and J1522−5735, the timing analysis reveals the presence of glitches, manifested as abrupt changes of the stars' rotation rates. These significantly complicate the timing procedure: if not additionally accounted for, they can lead to loss of phase-coherence.

In dedicated studies, we examined the spin-parameter changes associated with the glitches. For each of the two pulsars, we fixed the sky position to the pre-glitch timing solution, and scanned ranges in $\{f, \dot{f}\}$ on a dense grid around the pre-glitch spin parameters. At each grid point we computed the weighted H-test statistic (Kerr 2011) using photons within a fixed time window. This window was slid over the entire data set with 90% overlap between subsequent steps. The results are shown in Figure 2. The choice of time-window size balances signal-to-noise ratio and time resolution, being just long enough to still accumulate a detectable signal-to-noise ratio. These results enabled us to estimate values for the spin-parameter changes and glitch epochs for PSRs J1422−6138 and J1522−5735. We then iterated the timing procedure including a corresponding glitch model. The inferred glitch parameters are given in Table 1. In addition to permanent changes in f and $\dot{f}$, the glitch model for J1522−5735 also includes a frequency increment $\Delta f_{d,\mathrm{glitch\,1}}$ that decays exponentially on the timescale $\tau_{d,\mathrm{glitch\,1}}$ (Hobbs et al. 2006). Thus, the net effect after this spin-up glitch recovery is a spin-down, as shown in Figure 2(b).

Figure 3 shows the integrated pulse profiles and phase-time diagrams obtained from the full timing solutions. To characterize the profiles we fitted the observed gamma-ray light curves with combinations of Lorentzian and/or Gaussian lines. The complex pulse profile of PSR J0554+3107 was fitted using

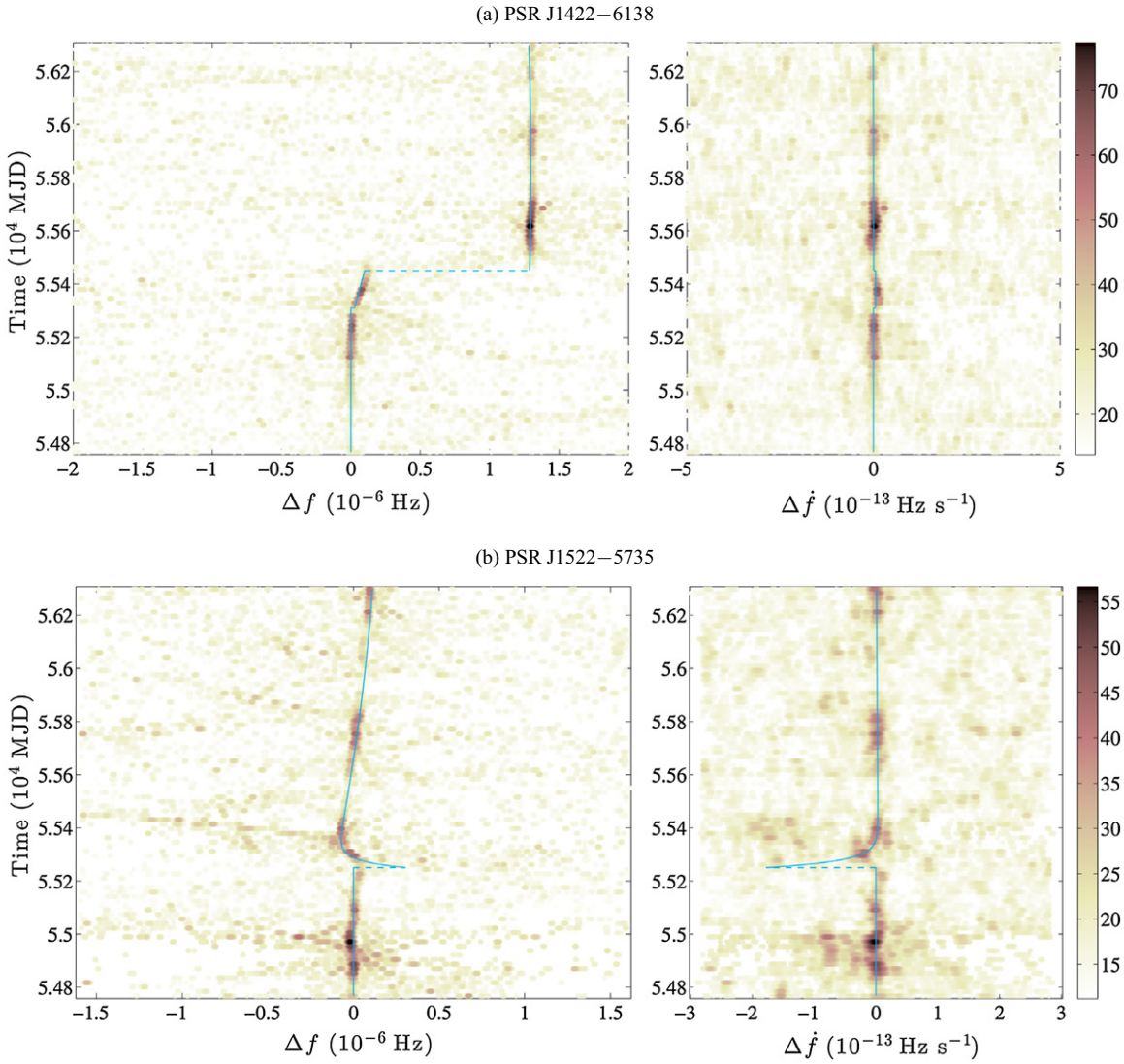

Figure 2. Pulsar glitch analyses for PSR J1422−6138 (a) and PSR J1522−5735 (b). The color code represents the weighted H-test using photons within a 170 day time window that is slid over the entire data set, with 90% overlap. At fixed (pre-glitch) sky position, for each window scans in H-test over $\{f, \dot{f}\}$ are done. Vertical axes show the time midpoint of each window. Horizontal axes show the offsets from the pre-glitch parameters in f (left), $\dot{f}$ (right). The solid blue curves are superimposed to show the timing solutions of Table 1.

(A color version of this figure is available in the online journal.)

asymmetric Lorentzian lines for the first two peaks, and a simple Gaussian for the last component. For PSR J1422−6138 the best fit is based on two simple Gaussian lines. For PSRs J1522−5735 and J1932+1916 we modeled the light curves with asymmetric Lorentzian lines. Table 1 shows the resulting peak separations and FWHMs.

We measured the pulsars' phase-averaged spectral properties through a binned likelihood analysis, using *pyLikelihood* of the STs. We constructed spectral models including all sources found within 20° of the pulsars from an internal catalog of gamma-ray sources based on 3 yr of LAT data, where the parameters only of point sources within 5° were left free. Each pulsar spectrum was modeled as an exponentially cut-off power law, $dN/dE \propto E^{-\Gamma} \exp(-E/E_c)$, where Γ denotes the spectral index and E_c is the cutoff energy. The source models included contributions from the Galactic diffuse emission (using model *gal_2yearp7v6_v0*), the extragalactic diffuse emission, and the residual instrumental background (using template *iso_p7v6source*[12]). For PSR J1422−6138, the phase-averaged analysis could not constrain Γ. Excluding "off-pulse" photons with phases between 0.55 and 0.95 (Figure 3) slightly improved the fit quality. The best-fit values for Γ, E_c, and the derived photon and energy fluxes are given in Table 1. These are in line with Γ and E_c values of other young LAT pulsars (Abdo et al. 2013), apart from PSR J1422−6138's low Γ which is currently not well constrained. Future LAT-event-reconstruction enhancements (Atwood et al. 2013) and more photon data may improve the latter measurement.

4. RADIO COUNTERPART SEARCHES

We searched for radio pulsations from the new gamma-ray pulsars with the Effelsberg and Parkes Telescopes. PSRs J0554+3107 and J1932+1916 were observed with the Effelsberg Telescope at 1.4 GHz for 1 hr, using the new

[12] http://fermi.gsfc.nasa.gov/ssc/data/access/lat/BackgroundModels.html

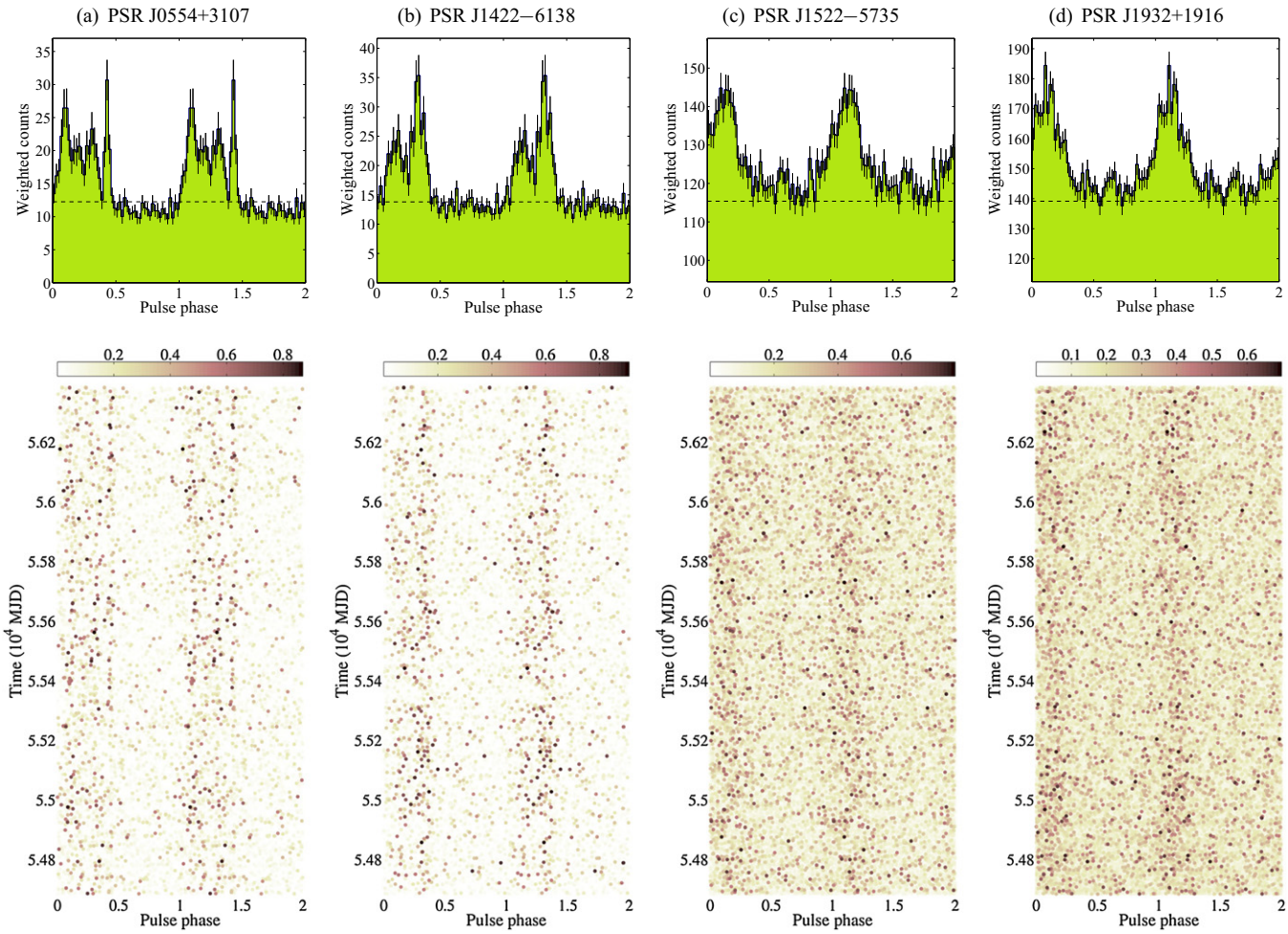

Figure 3. Top row: gamma-ray pulse profiles using the probability weights for photons with energies above 100 MeV. Each bin is 0.02 in rotation phase. Error bars represent 1σ statistical uncertainties. The dashed line indicates the estimated background level computed from the weights as in Guillemot et al. (2012). Each plot shows two pulsar rotations for clarity. Absolute phase references are arbitrarily set to 0.1 for the first peak. Bottom row: the pulsar rotational phase for each gamma-ray-photon arrival time; photon weights are shown in color code.

(A color version of this figure is available in the online journal.)

Ultra Broad Band (UBB) receiver (R. Keller et al. 2013, in preparation), as part of the commissioning of the instrument. For PSR J1422−6138, we used four 72 minute pointings taken during the High Time Resolution Universe survey (Keith et al. 2010), which we combined and searched coherently for increased sensitivity. Finally, for PSR J1522−5735 we analyzed a 2.4 hr Parkes observation. We used the gamma-ray pulsar ephemerides (Table 1), valid for each radio observation, to fold the radio data and searched in dispersion measure up to 2000 pc cm^{-3}.

We found no significant detection and provide upper limits on the radio flux density, derived with the modified radiometer equation (Lorimer & Kramer 2005) assuming a detection signal-to-noise-ratio threshold of 5 and a 10% duty cycle. Configuration details for the Parkes observations are found in Table 5 of Pletsch et al. (2012a). The observation of PSR J1522−5735 pointed 1.′5 away from the pulsar. This implies only a small sensitivity loss, because the beam's half-width at half-maximum is 7′ at this frequency. We accounted for this loss as in Pletsch et al. (2012a). For the 1.4 GHz Effelsberg observations, we assumed $n_p = 2$, $\beta = 1.2$, and a system equivalent flux density $T_{\rm sys}/G = 40.5$ Jy, as measured from preliminary UBB performance estimates[13] from continuum observations of 3C 48. After removal of radio-frequency interference, the nominal frequency bandwidth of 260 MHz was reduced to 225 and 205 MHz for PSRs J0554+3107 and J1932+1916, respectively. Table 1 lists the resulting radio-flux-density limits S_{1400} at 1.4 GHz, which are at the higher end compared to other LAT-discovered pulsars (e.g., Abdo et al. 2013). Although, assuming "heuristic" distances d_h (Table 1), the luminosities $S_{1400}\, d_h^2$ are lower than for the vast majority of known pulsars, deeper radio searches are possibly warranted to confirm the present picture.

5. DISCUSSION

The measured spin parameters of all four new gamma-ray pulsars classify them as young and energetic (Figure 1). Their spin-down powers, $\dot{E} = -4\pi^2 I f \dot{f}$, range from 5.6×10^{34} to 1.2×10^{36} erg s^{-1}, for an assumed neutron-star moment of inertia of $I = 10^{45}$ g cm^2. With characteristic ages τ_c between 35 and 56 kyr, they are among the youngest 4% of pulsars known (Manchester et al. 2005).[14]

The distances to the four new objects are difficult to constrain without detected radio pulsations providing a dispersion measure. However, an estimated upper bound for the

[13] UBB performance estimates may evolve as commissioning continues.

[14] http://www.atnf.csiro.au/research/pulsar/psrcat/

distance d to each pulsar can be obtained from relating $\dot{E}$ and the gamma-ray luminosity, $L_\gamma = 4\pi\, d^2\, f_\Omega\, G_{100}$, where f_Ω is a beam correction factor (Watters et al. 2009). Assuming 100% conversion efficiency ($L_\gamma = \dot{E}$) as an upper limit, and $f_\Omega \sim 1$, typical of gamma-ray pulsars (Watters et al. 2009), the above relation can then be solved for distance, which we denote by $d_{100\%}$. The resulting $d_{100\%}$ upper limits for the four pulsars are between 5 and 12 kpc. More realistically, if instead a "heuristic" gamma-ray luminosity (as in Abdo et al. 2013), $L^h_\gamma = (\dot{E}/10^{33}\ \mathrm{erg\ s^{-1}})^{1/2}\ 10^{33}\ \mathrm{erg\ s^{-1}}$ is assumed, distances between 1.5 and 2.1 kpc result (Table 1), suggesting that the pulsars are rather close.

Pulsars are believed to form in supernovae, so the discovery of a young pulsar prompts us to look for an associated supernova remnant (SNR). From Green (2009), we find a co-located SNR for two of the newly discovered pulsars. Care should be taken to establish genuine pulsar/SNR associations, because a chance superposition on the sky has a non-negligible probability (e.g., Gaensler & Johnston 1995; Kaspi 1998).

The sky position of PSR J0554+3107 lies about 6′ from the geometric center of SNR G179.0 + 2.6, which has an angular size of 70′ (Fuerst & Reich 1986). The low surface brightness Σ reported by Fuerst & Reich (1986) suggests a large SNR age of 10–100 kyr, which is compatible with the pulsar's characteristic age $\tau_c = 52$ kyr. This is a good estimator of the pulsar's true age if (1) the present spin period ($P = 465$ ms) is much larger than at birth and (2) the spin-down is dominated by magnetic dipole braking. From the Σ–diameter relation (Milne 1979), an SNR size of ≈70 pc yields a distance of ≈3.5 kpc. This has a large uncertainty, but is compatible with our estimated maximum pulsar distance $d_{100\%} = 5.2$ kpc. Depending on the estimated age and distance of the SNR, the required transverse velocity of PSR J0554+3107 is between 60 and 850 km s^{-1}, which is within the typical range of other pulsars (e.g., Hobbs et al. 2005). Thus it appears plausible that PSR J0554+3107 and G179.0 + 2.6 are associated.

The 102 ms pulsar J1522−5735 is located about 11′ from the centroid of SNR G321.9 − 0.3, which has an extension of 31′ × 23′. Caswell et al. (1975) provide an estimated distance of 5.5 kpc, compatible with our $d_{100\%} = 12.5$ kpc estimated upper limit for PSR J1522−5735. Their SNR age estimate of 20–100 kyr is also compatible with the $\tau_c = 52$ kyr characteristic age of PSR J1522−5735, given the same caveats as above. From the possible values of the estimated SNR age and distance, the necessary transverse speed of PSR J1522−5735 is between 170 and 860 km s^{-1}, which is also reasonable. Thus, a genuine association between PSR J1522−5735 and G321.9 − 0.3 is plausible and merits further study.

6. CONCLUSION

We have reported the Einstein@Home discovery and follow-up study of four gamma-ray pulsars found in a novel blind-search effort using *Fermi*-LAT data. The inferred parameters characterize the pulsars as energetic and young, likely relatively nearby. Young neutron stars are rare, and nearby ones in particular (e.g., Keane & Kramer 2008). As such, these four discoveries contribute toward a more complete understanding of the young pulsar population and neutron-star birthrates (Watters & Romani 2011). For two of the new pulsars, we have shown that associations with positionally coincident SNRs are possible. However, confirmation requires further work (e.g., measuring pulsar proper motion, a difficult task using LAT data alone).

All four gamma-ray pulsars lie close to the Galactic plane and remained undetected in subsequent targeted radio searches. In part, this is not unexpected, as argued by Camilo et al. (2012), since the vast majority of Galactic-plane (non-MSP) radio pulsars detectable by current radio telescopes and producing gamma-ray fluxes observable at Earth are likely already known. In turn, this demonstrates the importance of continued blind pulsar searches of gamma-ray data: it is the only way to discover such neutron stars. It is also remarkable that PSRs J1422−6138 and J1522−5735 have been detected in the blind search despite their prominent glitch activity. These facts, plus the combination of improved search techniques and massive Einstein@Home computing power leaves us optimistic that we can find more pulsars among the LAT unidentified sources.

We thank all Einstein@Home volunteers, and especially those whose computers detected the pulsars with the highest significance: PSR J0554+3107: "David Z," Canada, and "Test," France; PSR J1422−6138: Thomas M. Jackson, Kentucky, USA, and "mak-ino," Japan; PSR J1522−5735: NEMO computing cluster, UW-Milwaukee, USA, and "Chen," USA; PSR J1932+1916: Doug Lean, Australia, and Hans-Peter Tobler, Germany.

This work was supported by the Max-Planck-Gesellschaft (MPG). The *Fermi* LAT Collaboration acknowledges support from several agencies and institutes for both development and the operation of the LAT as well as scientific data analysis. These include NASA and DOE in the United States, CEA/Irfu and IN2P3/CNRS in France, ASI and INFN in Italy, MEXT, KEK, and JAXA in Japan, and the K. A. Wallenberg Foundation, the Swedish Research Council and the National Space Board in Sweden. Additional support from INAF in Italy and CNES in France for science analysis during the operations phase is also gratefully acknowledged. The UBB receiver construction was supported by the ERC under contract No. 279702. Einstein@Home is supported by the MPG and by US National Science Foundation grants 1104902 and 1105572.

REFERENCES

Aasi, J., Abadie, J., Abbott, B. P., et al. 2013, PhRvD, 87, 042001
Abbott, B. P., Abbott, R., Adhikari, R., et al. 2009a, PhRvD, 80, 042003
Abbott, I., Adams, M., Agari, M., et al. 2009b, PhRvD, 79, 022001
Abdo, A. A., Ackermann, M., Ajello, M., et al. 2009, Sci, 325, 840
Abdo, A. A., Ackermann, M., Ajello, M., et al. 2010, ApJS, 188, 405
Abdo, A. A., Ajello, M., Allafort, A., et al. 2013, ApJS, 208, 17
Ackermann, M., Ajello, M., Allafort, A., et al. 2012, ApJ, 753, 83
Allen, B., Knispel, B., Cordes, J. M., et al. 2013, ApJ, 773, 91
Atwood, W., Albert, A., Baldini, L., et al. 2013, arXiv:1303.3514
Atwood, W. B., Abdo, A. A., Ackermann, M., et al. 2009, ApJ, 697, 1071
Atwood, W. B., Ziegler, M., Johnson, R. P., & Baughman, B. M. 2006, ApJL, 652, L49
Brady, P. R., & Creighton, T. 2000, PhRvD, 61, 082001
Brady, P. R., Creighton, T., Cutler, C., & Schutz, B. F. 1998, PhRvD, 57, 2101
Camilo, F., Kerr, M., Ray, P. S., et al. 2012, ApJ, 746, 39
Caswell, J. L., Clark, D. H., Crawford, D. F., & Green, A. J. 1975, AuJPh, 37, 1
Chandler, A. M., Koh, D. T., Lamb, R. C., et al. 2001, ApJ, 556, 59
Cutler, C., Gholami, I., & Krishnan, B. 2005, PhRvD, 72, 042004
de Jager, O. C., Raubenheimer, B. C., & Swanepoel, J. W. H. 1989, A&A, 221, 180
Fuerst, E., & Reich, W. 1986, A&A, 154, 303
Gaensler, B. M., & Johnston, S. 1995, MNRAS, 275, L73
Green, D. A. 2009, BASI, 37, 45
Guillemot, L., Johnson, T. J., Venter, C., et al. 2012, ApJ, 744, 33
Hobbs, G., Lorimer, D. R., Lyne, A. G., & Kramer, M. 2005, MNRAS, 360, 974
Hobbs, G. B., Edwards, R. T., & Manchester, R. N. 2006, MNRAS, 369, 655
Kaspi, V. M. 1998, AdSpR, 21, 167
Keane, E. F., & Kramer, M. 2008, MNRAS, 391, 2009

Keith, M. J., Jameson, A., van Straten, W., et al. 2010, MNRAS, 409, 619
Kerr, M. 2011, ApJ, 732, 38
Knispel, B., Allen, B., Cordes, J. M., et al. 2010, Sci, 329, 1305
Knispel, B., Eatough, R. P., Kim, H., et al. 2013, ApJ, 774, 93
Knispel, B., Lazarus, P., Allen, B., et al. 2011, ApJL, 732, L1
Lee, K. J., Guillemot, L., Yue, Y. L., Kramer, M., & Champion, D. J. 2012, MNRAS, 424, 2832
Lorimer, D. R., & Kramer, M. 2005, in Handbook of Pulsar Astronomy, (Cambridge: Cambridge Univ. Press),
Manchester, R. N., Hobbs, G. B., Teoh, A., & Hobbs, M. 2005, AJ, 129, 1993
Milne, D. K. 1979, AuJPh, 32, 83
Nolan, P. L., Abdo, A. A., Ackermann, M., et al. 2012, ApJS, 199, 31
Pletsch, H. J. 2010, PhRvD, 82, 042002
Pletsch, H. J. 2011, PhRvD, 83, 122003
Pletsch, H. J., & Allen, B. 2009, PhRvL, 103, 181102
Pletsch, H. J., Guillemot, L., Allen, B., et al. 2012a, ApJ, 744, 105
Pletsch, H. J., Guillemot, L., Allen, B., et al. 2012c, ApJL, 755, L12
Pletsch, H. J., Guillemot, L., Fehrmann, H., et al. 2012b, Sci, 338, 1314
Ray, P. S., Abdo, A. A., Parent, D., et al. 2012, arXiv:1205.3089
Ray, P. S., Kerr, M., Parent, D., et al. 2011, ApJS, 194, 17
Romani, R. W. 2012, ApJL, 754, L25
Saz Parkinson, P. M., Dormody, M., Ziegler, M., et al. 2010, ApJ, 725, 571
Watters, K. P., & Romani, R. W. 2011, ApJ, 727, 123
Watters, K. P., Romani, R. W., Weltevrede, P., & Johnston, S. 2009, ApJ, 695, 1289
Ziegler, M., Baughman, B. M., Johnson, R. P., & Atwood, W. B. 2008, ApJ, 680, 620